A nonlinear bilayer beam model for an interfacial crack in dielectric bimaterials under mechanical/electrical loading

MingHao Zhao, HaiTao Liu, CuiYing Fan, Ernian Pan & Tong-Yi Zhang

International Journal of Fracture

ISSN 0376-9429
Volume 188
Number 1

Int J Fract (2014) 188:47-58
DOI 10.1007/s10704-014-9944-6


CODEN IJFRAP ISSN 0376-9429

international journal of fracture

Volume 188, No. 1, July 2014

TABLE OF CONTENTS

K. Ravi-Chandar, Editor-in-Chief
The University of Texas at Austin

Springer

NO AUTHOR CHARGES FOR COLOR PRINTING

Published since 1965

Springer

Int J Fract (2014) 188:47–58
DOI 10.1007/s10704-014-9944-6

ORIGINAL PAPER

A nonlinear bilayer beam model for an interfacial crack in dielectric bimaterials under mechanical/electrical loading

MingHao Zhao · HaiTao Liu · CuiYing Fan · Ernian Pan · Tong-Yi Zhang

Received: 9 November 2013 / Accepted: 1 April 2014 / Published online: 10 April 2014

Abstract A bilayer beam model is extended to study the fracture behavior of dielectric interfacial cracks. In this model, a semi-infinite crack with an original opening value is oriented along the interface between two dielectric layers which are under mechanical/electrical loading. Taking into account the effect of the electrostatic traction on the interfacial crack, a nonlinear analytical solution is derived, along with also a developed finite element analysis method where a special constitutive equation for the capacitor element in ANSYS is utilized to simulate the electrostatic tractions. Both the analytical and numerical solutions predict the same results which further show that the elastic and dielectric mismatches can play a significant role in the interfacial cracking behavior under mechanical and electrical loading. Furthermore, the electrostatic tractions may cause hysteresis loops in the curve of crack opening versus applied mechanical displacement or versus applied electric voltage. An applied mechanical load is the driving force for the interfacial cracking, while an applied electric field retards it.

M. Zhao · C. Fan (✉) · E. Pan
Henan Key Engineering Laboratory for Anti-fatigue Manufacturing Technology and School of Mechanical Engineering, Zhengzhou University,
No. 100 Science Road, Zhengzhou 450001, Henan, People's Republic of China
e-mail:fancy@zzu.edu.cn

M. Zhao · H. Liu
School of Mechanics and Engineering Science, Zhengzhou University, Zhengzhou 450001,
Henan, People's Republic of China
e-mail:memhzhao@zzu.edu.cn

T.-Y. Zhang
Department of Mechanical and Aerospace Engineering, Hong Kong University of Science and Technology, Clear Water Bay, Kowloon, Hong Kong,
People's Republic of China

Keywords Bilayer beam model · Dielectric bimaterials · Electrostatic traction · Nonlinear analytical solution · TRANS126 element · Interfacial fracture

1 Introduction

Debonding is one of the common failure modes in composite materials. The study of interfacial crack began about 60 years ago (e.g., Cherepanov 1962; England 1965; Erdogan 1965; Rice and Sih 1965, etc.). The bilayer beam model is one of the most important ones widely used in the calibration of interfacial fracture toughness of layered materials and structures (e.g., Tada et al. 1985; Williams 1988; Suo and Hutchinson 1989; Shapery and Davidson 1990; Suo 1990). The problem of a homogeneous layer with a crack located on the mid-plane with rigid grips, as shown in Fig. 1, was solved analytically by Rice in 1968. Liechti and Chai (1990) studied the mixed mode interfacial fracture problem using a gripped bilayer beam model. A detailed review on the bilayer beam fracture model was given by Hutchinson and Suo (1992). The advantage of

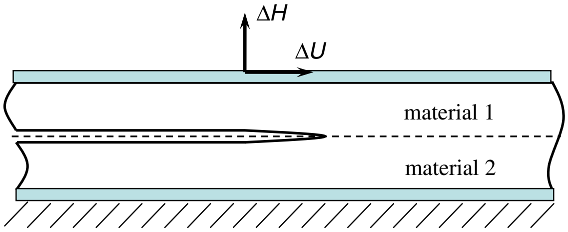

Fig. 1 Schematic diagram of the bilayer beam fracture model

such a beam fracture model is that the energy release rate calculated is completely independent of the crack tip location and is determined only by the difference between the energy far ahead of the crack tip and that far behind the crack tip. Thus, the energy release rate in this model can be analytically and simply expressed in terms of the elastic material properties and the geometric parameters, avoiding the evaluation of the local field variables at the crack tip. Furthermore, the analytical solution can be easily utilized to extract the interfacial fracture toughness by using the bilayer beam fracture model experiment.

Because of its coupled mechanical and electric properties, dielectric/piezoelectric materials have been widely used in intelligent structures and systems, such as sensors or actuators. Meanwhile, multi-layered structures are often preferred in the manufacture of composite materials and are widely used in engineering to enhance the efficiency and sensitivity of materials or structures. Thus, for the safety of smart structures, it is necessary to study the interface fracture of dielectric/piezoelectric material. However, such an extension is never simple, taking for example, on the treatment of the boundary condition on crack face. Because the dielectric constant inside the crack differs to that in the surrounding material, electric charges will be induced along the crack faces when an electric field is applied. Therefore, the influence of electric boundary condition on the fracture of electrically insulating cracks in dielectric and piezoelectric materials under mechanical-electric loading are important as was previously reported (e.g., Zhang and Hack 1992; Suo et al. 1992; Hao and Shen 1994; Zhang et al. 1998; Zhang and Gao 2004; McMeeking 2004; Gao et al. 2004b; Landis 2004; Schneider 2007; Li and Chen 2008). Gao et al. (2004a) estimated the electrostatic force between the induced charges on the two crack faces and analyzed the effect of the electrostatic force on the fracture behavior. If one takes the electrostatic traction along the crack faces as a mechanical boundary condition, then the traction-free boundary condition along the crack faces does not hold any more. Ricoeur and Kuna (2009) developed a general relation describing electrostatic stresses on the interface between dielectric bodies exposed to electric fields. The derivation was based on the thermodynamic consideration of the electromechanical system, which leads to a formulation of the configurational forces acting on the interface.

To fully understand the effect of the electrostatic tractions on the fracture behavior, Zhang and Xie (2012) developed a pre-cracked parallel-plate capacitor model, in which an infinitely long beam of a dielectric material containing a semi-infinite crack with an original crack opening value is under mechanical and/or electric loading. In their model, the dielectric material is sandwiched between two rigid electrodes, and therefore, the electrostatic tractions along the dielectric/electrode interfaces can be considered. This model allows one to obtain solution analytically in a straightforward way. Their results (Zhang and Xie 2012) indicated that the fracture problem might be converted into an electrically sticky problem if the electrostatic tractions are high enough. They also found the hysteresis loops in both curves of crack opening displacement versus the applied electric field or versus the applied mechanical load. The mechanical load is the driving force to propagate the crack, while the applied electric field retards crack propagation due to the electrostatic tractions. Furthermore, the fracture criterion is composed of two parts: the energy release rate must exceed a critical value and the mechanical load must be higher than the critical value for crack opening. Xie et al. (2014) further developed the pre-cracked parallel-plate capacitor model for piezoelectric materials.

Following Zhang and Xie (2012) and Hutchinson and Suo (1992), we study, in the present paper, the effects of the electrostatic tractions on the interfacial fracture behavior of a bimaterial by using the extended bilayer beam fracture model, shown in Fig. 2. A semi-infinite crack is located along the interface between the two layers, which have different dielectric and elastic properties. The pre-cracked bilayer beam is sandwiched between two rigid electrodes, and mechanical and electric loads are applied on the electrodes. As charges will be induced along the crack faces when an electric field is applied, the electrostatic force between the induced charges on the two crack faces will be con-

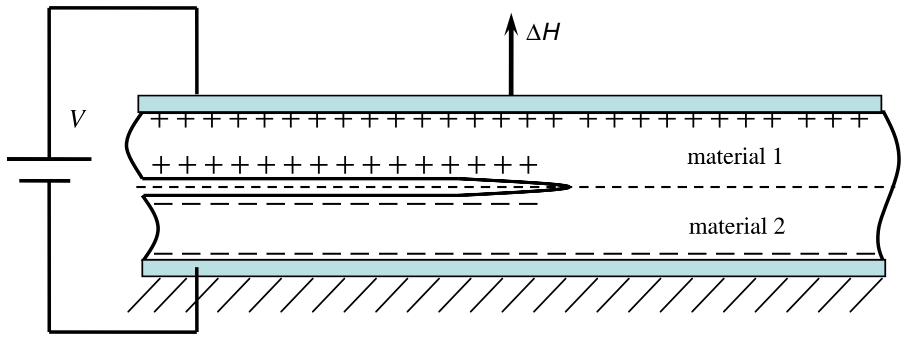

Fig. 2 Schematic diagram of the bilayer beam fracture model applied by combined mechanical-electrical loading

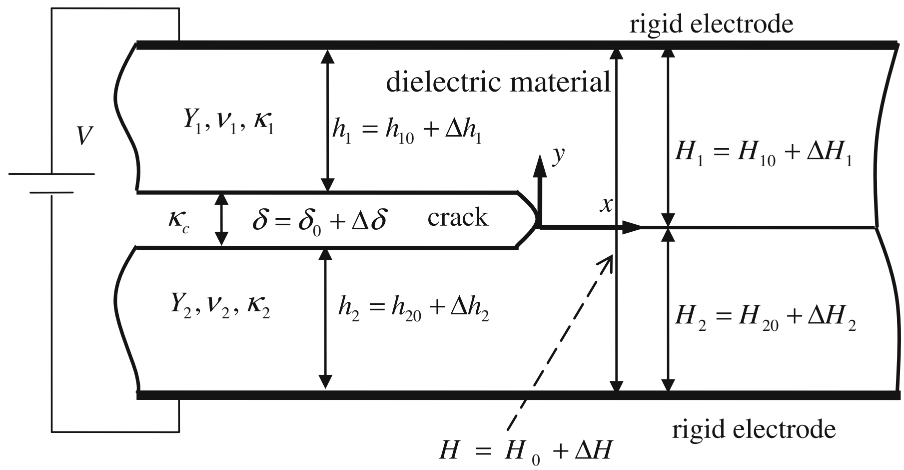

Fig. 3 A pre-cracked bilayer beam under mechanical and electric loading

sidered in the study. For simplicity, the layer materials are dielectric following isotropic and linear constitutive equations such that analytic solutions can be derived from the proposed model. This paper is organized as follows. After the introduction, Sect. 2 describes the bilayer beam model and the analytical derivation. A finite element model for the bilayer beam with the electrostatic traction is presented in Sect. 3. Numerical examples are given in Sect. 4, and conclusions are drawn in Sect. 5.

2 A nonlinear bilayer beam model

Figure 3 shows a bilayer beam between two rigid electrodes, in which there is a semi-infinite interfacial notch or crack. Before applying the voltage or the displacement loading, the thickness of each layer in the uncracked part is denoted by H_{i0}, where $i = 1$ and 2 indicate the upper and lower layer, respectively. In the pre-cracked part, the thickness of each layer is reduced to h_{i0} due to the notch width δ_0. In the present paper, we take $h_{10}/h_{20} \equiv H_{10}/H_{20}$. Each layer is homogenous, with the Young's modulus, Poisson's ratio and the dielectric constant being denoted, respectively, by Y_i, ν_i and κ_i.

A Cartesian coordinate system oxy is attached to the bilayer beam such that the origin o coincides with the tip of the notch and the x-axis is along the interface. An electric voltage V and a relative mechanical displacement ΔH are applied on the two rigid electrodes. Thereafter, ΔH is also called the mechanical load. Due to the applied loads, each layer changes its thickness by ΔH_i in front of the crack tip and by Δh_i behind the crack tip such that

$$h_i = h_{i0} + \Delta h_i, \tag{1a}$$

$$H_i = H_{i0} + \Delta H_i, \tag{1b}$$

$$\Delta H = \Delta H_1 + \Delta H_2. \tag{1c}$$

When the mechanical displacement ΔH and the electric voltage V are independent variables, the electric enthalpy, P, will be the appropriate thermodynamics function. In the differential form, we have

$$dP = Fd(\Delta H) - QdV, \tag{2}$$

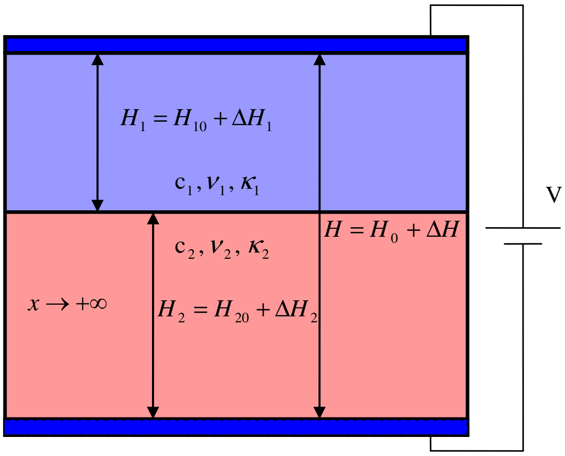

Fig. 4 Beam segment far ahead of the crack tip $x \to +\infty$, showing the perfectly bounded bilayer beam

where F denotes the mechanical force and Q the electric charge.

Far ahead the crack tip, $x \to +\infty$, the configuration can be treated as two parallel-plate capacitors in series, as shown in Fig. 4. For this plane strain problem, it is assumed that the displacement in the x-direction is negligible. Thus, the following conditions must be satisfied on the upper surface of layer 1 ($i = 1$) and lower surface of layer 2 ($i = 2$):

$$\sigma_{\mathrm{E}i}^{+} + \sigma_{\mathrm{M}i}^{+} \equiv \sigma_i^{+} = c_i \varepsilon_i^{+}, \tag{3}$$

$$q_i^{+} \equiv D_i^{+} = \kappa_i E_i^{+}, \tag{4}$$

here and hereafter, the superscript "+" is used exclusively for the fields at $x \to +\infty$. Also in Eqs. (3) and (4), $c_i = \frac{1-\nu_i}{(1+\nu_i)(1-2\nu_i)} Y_i$, $\sigma_{\mathrm{M}i}^{+}$ and $\sigma_{\mathrm{E}i}^{+}$denotes the stresses induced by the mechanical loading and the electric loading, respectively. σ_i^{+}, ε_i^{+}, q_i^{+}, $\mathrm{D}_i^{+}$and E_i^{+} are the stress, strain, density of the electric charges, electric displacement and the electric field strength in each layer, respectively, which are calculated by

$$\varepsilon_i^{+} = \frac{\Delta H_i}{H_{i0}}, \tag{5}$$

$$E_i^{+} = -\frac{V_i^{+}}{H_i}, \tag{6}$$

where V_i^{+} is the electric voltage between the two surfaces of each layer.

Along the interface, $y = 0$, between the two layers, the mechanical balance requires

$$c_1 \varepsilon_1^{+} + t_E^{+} = c_2 \varepsilon_2^{+}, \tag{7}$$

where t_E^{+} is the electrostatic tractions on the interface given by Ricoeur and Kuna (2009)

$$t_{\mathrm{E}}^{+} = \frac{1}{2} D^{+}(E_1^{+} - E_2^{+}), \tag{8}$$

In Eq. (8), $D^{+}$is the continuous electric displacement across the interface ($y = 0$)

$$D_1^{+} = \kappa_1 E_1^{+},\ D_2^{+} = \kappa_2 E_2^{+}, \tag{9a}$$

$$D^{+} = D_1^{+} = D_2^{+}. \tag{9b}$$

The potential drops across the two layers satisfy

$$V_1^{+} + V_2^{+} = V. \tag{10}$$

Solving Eqs. (6), (9) and (10) yields

$$E_1^{+} = -\frac{\kappa_2 V}{\kappa_1 H_2 + \kappa_2 H_1},\quad E_2^{+} = -\frac{\kappa_1 V}{\kappa_2 H_1 + \kappa_1 H_2}. \tag{11}$$

Substituting Eq. (11) into Eq. (9) and then into Eq. (8), we obtain the electrostatic tractions in terms of the applied voltage V, thicknesses H_i and the dielectric constants κ_i of the two layers

$$t_E^{+} = \frac{(\kappa_2 - \kappa_1)\kappa_1 \kappa_2 V^2}{2(\kappa_1 H_2 + \kappa_2 H_1)^2}. \tag{12}$$

Substituting Eq. (12) into Eq. (7) gives

$$c_1 \frac{\Delta H_1}{H_{10}} - c_2 \frac{\Delta H_2}{H_{20}} = -\frac{(\kappa_2 - \kappa_1)\kappa_1 \kappa_2 V^2}{2(\kappa_1 H_2 + \kappa_2 H_1)^2}. \tag{13}$$

If $\kappa_1 = \kappa_2$, the dielectric mismatch disappears and there is no electrostatic tractions on the interface. Then, Eq. (13) is reduced to

$$c_1 \frac{\Delta H_1}{H_{10}} - c_2 \frac{\Delta H_2}{H_{20}} = 0. \tag{14}$$

Solving Eqs. (1) and (14) gives

$$\Delta H_1 = \frac{c_2 H_{10}}{c_1 H_{20} + c_2 H_{10}} \Delta H,$$

$$\Delta H_2 = \frac{c_1 H_{20}}{c_1 H_{20} + c_2 H_{10}} \Delta H. \tag{15}$$

In this case, the deformation of each layer is independent of the applied electric load.

When $\kappa_1 \neq \kappa_2$, substituting Eq. (1c) into Eq. (13), we obtain the following cubic equation for $(\Delta H_1/H_{10})$

$$(\Delta H_1/H_{10})^3 + e_2 (\Delta H_1/H_{10})^2$$
$$+e_1 (\Delta H_1/H_{10}) + e_0 = 0, \tag{16}$$

where the coefficients e_2, $e_1$and e_0 are given by

$$e_2 = 2d_2 - d_1,$$
$$e_1 = -2d_1 d_2 + (d_2)^2,$$
$$e_0 = -d_1 (d_2)^2 - d_3, \tag{17}$$

with

$$d_1 = \frac{c_2 \Delta H}{c_2 H_{10} + c_1 H_{20}}, \tag{18a}$$

$$d_2 = \frac{\kappa_1 (H_{20}/H_{10}) + \kappa_1 (\Delta H/H_{10}) + \kappa_2}{\kappa_2 - \kappa_1}, \tag{18b}$$

$$d_3 = \frac{\kappa_1 \kappa_2 V^2}{(\kappa_2 - \kappa_1)(H_{10}/H_{20})(c_2 H_{10} + c_1 H_{20}) H_{10}}. \tag{18c}$$

Solving Eq. (16) gives

$$\Delta H_1/H_{10} = \left[-\frac{e_0^*}{2} + \sqrt{\left(\frac{e_0^*}{2}\right)^2 + \left(\frac{e_1^*}{3}\right)^3} \right]^{\frac{1}{3}} + \left[-\frac{e_0^*}{2} - \sqrt{\left(\frac{e_0^*}{2}\right)^2 + \left(\frac{e_1^*}{3}\right)^3} \right]^{\frac{1}{3}} - \frac{e_2}{3}, \tag{19}$$

where

$$e_0^* = e_0 - \frac{e_1 e_2}{3} + 2\left(\frac{e_2}{3}\right)^3,$$

$$e_1^* = e_1 - 3\left(\frac{e_2}{3}\right)^2. \tag{20}$$

The other two roots of Eq. (16) have no physical meaning. From Eq. (19) and Eq. (1c), it can be seen that each layer can be deformed under mechanical and/or electric loadings.

Based on Eqs. (2)–(4), the electric enthalpy density in the upper or lower layer is given by

$$p_i^+ = \frac{1}{2}\sigma_i^+ \varepsilon_i^+ - \frac{1}{2} D_i^+ E_i^+, \tag{21}$$

where $i = 1$ and 2 indicate the upper and lower layer, respectively.

Thus, the electric enthalpy per unit length P^+ can be expressed as

$$P^+ = \frac{1}{2}\sigma_1^+ \varepsilon_1^+ H_1 - \frac{1}{2} D_1^+ E_1^+ H_1 + \frac{1}{2}\sigma_2^+ \varepsilon_2^+ H_2 - \frac{1}{2} D_2^+ E_2^+ H_2. \tag{22}$$

Similarly, far behind the crack tip, $x \to -\infty$, the two layers are separated by a notch gap, which can be considered as three parallel-plate capacitors in series with two dielectric parallel-plate capacitors and one vacuum parallel-plate capacitor, as shown in Fig. 5. The two dielectric parallel-plate capacitors have thickness h_1 and h_2, respectively, and the gap between them, called the notch width, is δ. The following conditions

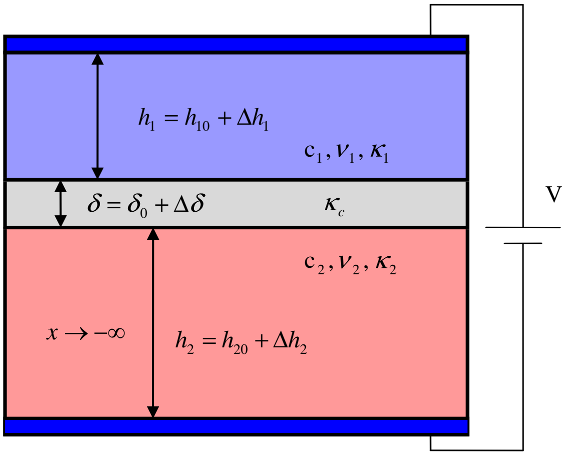

Fig. 5 Beam segment far behind the crack tip $x \to -\infty$, showing an interfacial crack with an original width between two dielectric layers

must be satisfied in each layer (hereafter, the superscript "-" is used exclusively for the quantities at $x \to -\infty$)

$$\sigma_{Ei}^- + \sigma_{Mi}^- \equiv \sigma_i^- = c_i \varepsilon_i^-, \tag{23}$$

$$q_i^- \equiv D_i^- = \kappa_i E_i^-. \tag{24}$$

The elastic strain, ε_i^-, electric field strengths in each layer, E_i^-, and inside the gap, E_c^-, are respectively calculated by

$$\varepsilon_i^- = \frac{\Delta h_i}{h_{i0}}, \tag{25}$$

$$E_i^- = -\frac{V_i^-}{h_i}, \quad E_c^- = -\frac{V_c^-}{\delta}, \tag{26}$$

where V_i^- and V_c^- are the potential drops across each layer and the gap, respectively, which satisfy the relation

$$V_1^- + V_c^- + V_2^- = V. \tag{27}$$

The electric displacement is continuous across the interfaces between the layers and the gap, which requires

$$D_1^- = \kappa_1 E_1^-, \quad D_2^- = \kappa_2 E_2^-, \quad D_c^- = \kappa_c E_c^-, \tag{28a}$$

$$D_1^- = D_2^- = D_c^- = D^-, \tag{28b}$$

where $\kappa_c$denotes the dielectric constant of the medium inside the gap. Solving Eqs. (26)–(28) yields

$$E_i^- = -\frac{V}{L_0}\frac{\kappa_c}{\kappa_i}, \quad E_c^- = -\frac{V}{L_0}, \tag{29}$$

where

$$L_0 = \frac{\kappa_c}{\kappa_1} h_1 + \frac{\kappa_c}{\kappa_2} h_2 + \delta. \tag{30}$$

Thus, we have the density of the electric charge

$$q^- \equiv D^- = -\kappa_c \frac{V}{L_0}. \tag{31}$$

The electrostatic traction on the bottom of layer 1 ($i = 1$) or on the top of layer 2 ($i = 2$) is given by Ricoeur and Kuna (2009)

$$t_i = (-1)^i \frac{1}{2}\frac{\kappa_c V^2}{L_0^2}\left(1 - \frac{\kappa_c}{\kappa_i}\right), \tag{32}$$

The mechanical force balance requires

$$(-1)^i t_i = c_i \frac{\Delta h_i}{h_{i0}} = c_i \frac{h_i - h_{i0}}{h_{i0}}. \tag{33}$$

Thus, we have

$$\frac{c_1 h_{20}(h_1 - h_{10})}{c_2 h_{10}(h_2 - h_{20})} = \frac{\kappa_2(\kappa_1 - \kappa_c)}{\kappa_1(\kappa_2 - \kappa_c)}. \tag{34}$$

Equation (34) can be rewritten as

$$\frac{h_1 - h_{10}}{h_2 - h_{20}} = R, \tag{35}$$

where R is a material and geometry related parameter defined as

$$R = \frac{c_2 h_{10}}{c_1 h_{20}} \frac{\kappa_1\kappa_2 - \kappa_2\kappa_c}{\kappa_1\kappa_2 - \kappa_1\kappa_c}. \tag{36}$$

Finally, we have

$$h_1 = R h_2 - R h_{20} + h_{10}, \tag{37}$$

$$\delta = H + R h_{20} - h_{10} - (R+1) h_2, \tag{38}$$

$$L_0 = \left(\frac{\kappa_c}{\kappa_1} - 1\right)(h_{10} - R h_{20}) + H + \left(\frac{\kappa_c}{\kappa_1} R + \frac{\kappa_c}{\kappa_2} - R - 1\right) h_2, \tag{39}$$

where Eq. (39) is obtained from Eq. (30) by using Eqs. (37) and (38). Substituting Eq. (39) into Eqs. (32) and (33) for $i = 2$, we obtain the following cubic equation for h_2

$$(h_2/h_{20})^3 + b_2 (h_2/h_{20})^2 + b_1 (h_2/h_{20}) + b_0 = 0, \tag{40}$$

where

$$b_0 = -a_1^2 - \frac{1}{2}\left(1 - \frac{\kappa_c}{\kappa_2}\right)\frac{\kappa_c V^2}{c_2 a_2^2 h_{20}^2},$$

$$b_1 = -2a_1 + a_1^2,$$

$$b_2 = 2a_1 - 1, \tag{41}$$

with

$$a_1 = \left(\frac{\kappa_c}{\kappa_1}(-R + h_{10}/h_{20}) + H/h_{20} + R - h_{10}/h_{20}\right)/a_2,$$

$$a_2 = \frac{\kappa_c}{\kappa_1} R + \frac{\kappa_c}{\kappa_2} - R - 1. \tag{42}$$

Solving Eq. (40) gives us the following three roots

$$h_2/h_{20} = \left[-\frac{b_0^*}{2} + \sqrt{\lambda}\right]^{\frac{1}{3}} + \left[-\frac{b_0^*}{2} - \sqrt{\lambda}\right]^{\frac{1}{3}} - \frac{b_2}{3}, \tag{43a}$$

$$h_2/h_{20} = \frac{-1 - i\sqrt{3}}{2}\left[-\frac{b_0^*}{2} + \sqrt{\lambda}\right]^{\frac{1}{3}} + \frac{-1 + i\sqrt{3}}{2}\left[-\frac{b_0^*}{2} - \sqrt{\lambda}\right]^{\frac{1}{3}} - \frac{b_2}{3}, \tag{43b}$$

$$h_2/h_{20} = \frac{-1 + i\sqrt{3}}{2}\left[-\frac{b_0^*}{2} + \sqrt{\lambda}\right]^{\frac{1}{3}} + \frac{-1 - i\sqrt{3}}{2}\left[-\frac{b_0^*}{2} - \sqrt{\lambda}\right]^{\frac{1}{3}} - \frac{b_2}{3}, \tag{43c}$$

where

$$b_0^* = b_0 - \frac{b_1 b_2}{3} + 2\left(\frac{b_2}{3}\right)^3,$$

$$b_1^* = b_1 - 3\left(\frac{b_2}{3}\right)^2,$$

$$\lambda = \left(\frac{b_0^*}{2}\right)^2 + \left(\frac{b_1^*}{3}\right)^3. \tag{44}$$

Detailed discussions about the three solutions were given in Fan et al. (2011) and Zhang and Xie (2012).

We discuss two special cases of the electric field associated with Eq. (40):

1. The electric field E_0 corresponding to the critical gap opening with

$$\delta = 0. \tag{45}$$

For this case, we can solve Eq. (40) for E (by letting $\delta = 0$, or substituting $h_2 = h_{20} + (\delta_0 + \Delta H)R/(R+1)$ into Eq. (40)) to find the corresponding electric field as

$$E_0 \equiv -\frac{V_0}{h_{10}} = \sqrt{\frac{2c_2}{(R+1)\kappa_c}\left(1 - \frac{\kappa_c}{\kappa_2}\right)\eta\tau\left[\xi\left(1 + \frac{R}{R+1}\tau\right) + \frac{\kappa_c}{\kappa_2}\left(\frac{1}{\eta} + \tau\right)\right]}, \tag{46}$$

where the dimensionless geometric parameters are defined by

$$\tau \equiv \frac{\delta_0 + \Delta H}{h_{10}}, \quad \eta = \frac{h_{10}}{h_{20}} \equiv \frac{H_{10}}{H_{20}}, \tag{47}$$

and the dielectric mismatch parameters are denoted by

$$\gamma = \frac{\kappa_1 - \kappa_2}{\kappa_1 + \kappa_2}, \quad \xi = \frac{\kappa_c}{\kappa_1}. \tag{48}$$

It can be seen that $E_0$is dependent on the material properties and geometric parameters, as well as on the mechanical loading via τ. In general, we have $\xi << 1, \tau << 1, \eta \sim 1$, and $\gamma \sim 1$, and thus Eq. (46) is simplified to

$$E_0 \equiv \sqrt{\frac{2c_2}{(R+1)\kappa_c}\eta\tau}\left[\xi + \frac{\kappa_c}{\kappa_2}\frac{1}{\eta}\right]. \tag{49}$$

2. The electric field E_{max} (which is also the maximum tolerant value) corresponding to the threshold in the $\delta - E$ curve. For this case, we take the derivative of Eq. (40) with respect to E (i.e., taking the derivative of δ with respect to E), and let the result equals zero, which gives us

$$E_{\max} \equiv \sqrt{\frac{2c_2}{(R+1)\kappa_c}\left(1-\kappa_c/\kappa_2\right)\eta k}\left[\xi\left(1+\frac{R}{R+1}k\right) + \frac{\kappa_c}{\kappa_2}\left(\frac{1}{\eta}+\frac{1}{R+1}k\right)+\tau-k\right], \tag{50}$$

where the dimensionless parameter is given by

$$k = \frac{\xi + \kappa_c/(\eta\kappa_2) + \tau}{3\left[\xi R/(R+1) + \kappa_c/[(R+1)\kappa_2] - 1\right]}. \tag{51}$$

Similar to E_0, $E_{\max}$ depends on the material properties and geometric parameters, as well as on the mechanical loading via τ. Generally, Eq. (50) can be simplified to

$$E_{\max} \equiv \sqrt{\frac{2c_2}{(R+1)\kappa_c}\eta k}\left[\xi + \frac{\kappa_c}{\kappa_2}\frac{1}{\eta} + \tau - k\right]. \tag{52}$$

It is easily to show that $E_0 \le E_{\max}$. These solutions for E_0 and $E_{\max}$ will be plotted and discussed in Sect. 4.

Similar to Eq. (22), the electric enthalpy per unit length, P^- at the location far behind the crack tip, i.e., $x \to -\infty$, can be also expressed as

$$P^- = \frac{1}{2}\sigma_1^- \varepsilon_1^- h_1 - \frac{1}{2}D^- E_1^- h_1 + \frac{1}{2}\sigma_2^- \varepsilon_2^- h_2 - \frac{1}{2}D^- E_2^- h_2 - \frac{1}{2}D^- E_c^- \delta. \tag{53}$$

It should be pointed out that without considering the electrostatic traction, the electric enthalpy expression in Eq. (53) will be reduced to

$$P^- = -\frac{1}{2}D^- E_1^- h_{10} - \frac{1}{2}D^- E_2^- h_{20} - \frac{1}{2}D^- E_c^- (\delta_0 + \Delta H). \tag{54}$$

Finally, combing Eqs. (22) and (53), we obtain the energy release rate as Hutchinson and Suo (1992)

$$\begin{aligned} G &= P^+ - P^- \\ &= \frac{1}{2}\sigma_1^+\varepsilon_1^+ H_1 - \frac{1}{2}D_1^+ E_1^+ H_1 \\ &\quad + \frac{1}{2}\sigma_2^+\varepsilon_2^+ H_2 - \frac{1}{2}D_2^+ E_2^+ H_2 - \frac{1}{2}\sigma_1^-\varepsilon_1^- h_1 \\ &\quad + \frac{1}{2}D^- E_1^- h_1 - \frac{1}{2}\sigma_2^-\varepsilon_2^- h_2 + \frac{1}{2}D^- E_2^- h_2 \\ &\quad + \frac{1}{2}D^- E_c^- \delta. \end{aligned} \tag{55}$$

3 Finite element model

In the commercial finite element software ANSYS there is an element TRANS126 called "reduced-order" element, which is used as a transducer in structural finite element simulations or as a transducer in "lumped" electromechanical circuit simulation. "Reduced-order" means that the electrostatic characteristics of an electromechanical device is captured in terms of the capacitance of the device over a range of displacements (or stroke of the device) and is further formulated in a simple coupled beam-like element (ANSYS® Academic Research, Element Reference). Figure 6a shows schematically a parallel-plate capacitor with the gap δ between the two plates. The parallel-plate capacitor can be reduced to a beam-like element and the electrostatic force between the electrodes can be simulated by the TRANS126 element in ANSYS. The element has two nodes, each with the degrees of freedom of UX-VOLT, UY-VOLT or UZ-VOLT as shown in Fig. 6b. Only the displacement in the gap direction is concerned. The capacitance C can be expressed in terms of the gap as

$$C = C_0/\delta + C_1 + C_2\delta + C_3\delta^2 + C_4\delta^3, \tag{56}$$

where C_i are the material/geometry related coefficients. Under an applied voltage, the electrostatic force between the electrodes can be calculated by

$$F = \frac{1}{2}V_c^2\frac{\mathrm{d}C}{\mathrm{d}\delta}, \tag{57}$$

where V_c is the voltage cross the electrodes. Assuming that the gap of the capacitor is small and also keeping only the first term in Eq. (56), the capacitance can be calculated by

$$C = \frac{\kappa_c A}{\delta}, \tag{58}$$

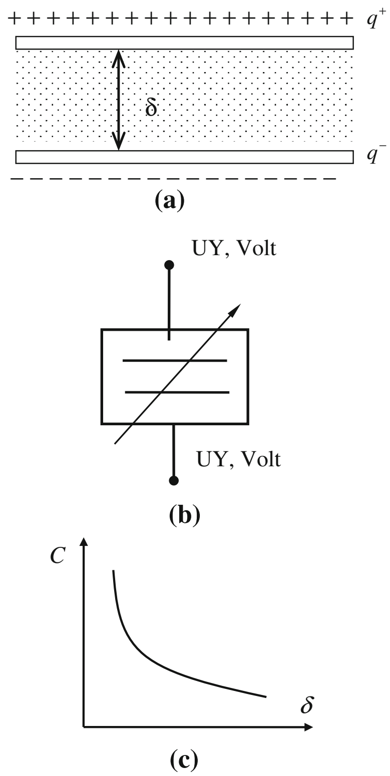

Fig. 6 TRANS126 element. **a** A parallel plate capacitor. **b** Electrostatic finite element model. **c** Capacitance C vs. δ curve

where κ_c is the dielectric constant of the material between the plates and A is the area of the plate. Figure 6c shows the typical curve of capacitance C vs. δ based on Eq. (58).

Substituting Eq. (58) into Eq. (57) yields

$$F/A = -\frac{\kappa_c}{2}\frac{V_c^2}{\delta^2} \quad . \tag{59}$$

It is interesting to observe that the traction per unit area given by Eq. (59) is the electrostatic traction acting on the crack faces when the dielectric material (in the case of $\kappa_c << \kappa_i$) is electrically and mechanically loaded (Landis 2004; Ricoeur and Kuna 2009; Zhang and Xie 2012). Thus, the TRANS126 element in ANSYS can be used to simulate the electrostatic traction acting on the crack faces. Figure 7 shows schematically the constitutive equation of TRANS126 element in ANSYS which is the relation of the force F vs. the distance δ between the two nodes. Also in this figure, GAPMIN is the critical gap. When the gap is less than GAPMIN, the element is degenerated to a contact element, with the stiffness denoted by KN. In this paper, however, we are not interested in the behavior once the gap shrinks to zero.

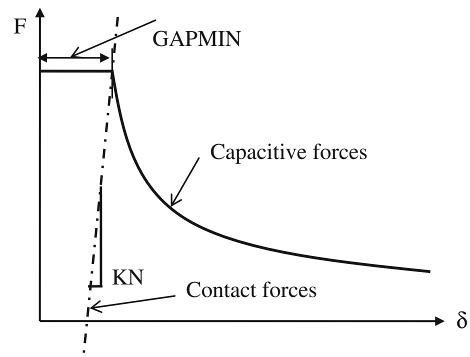

Fig. 7 Constitutive relationship of TRANS126 element

4 Results and discussion

Figure 8a shows the element meshes (with different zooms) of a bilayer beam model, where the quadrilateral element PLANE223 in ANSYS is used to simulate the electric field and the TRANS126 element described in the previous section to simulate the electrostatic tractions on the notch/crack surfaces. In the numerical analysis, the bilayer beam is 400mm in length and 40mm in width, and 16297 PLANE223 elements and 200 TRANS126 elements are used (Fig. 8a). The two cross sections at the two ends of the bilayer beam are subjected to roller support condition, and the bottom of the beam is fixed with zero electric potential. The displacement and electric loads are applied on the top of the bilayer beam. Figure 8b shows the stress distribution in the thickness direction of the beam by finite element analysis, where

$$\begin{aligned} &h_{10} = h_{20} = 20\,\text{mm}, \quad \delta_0 = 40\,\mu\text{m},\\ &Y_1 = 100\,\text{GPa}, \quad Y_2 = 50\,\text{GPa}, \quad \nu_1 = \nu_2 = 0.3,\\ &\xi = \kappa_c/\kappa_1 = 10^{-4},\\ &\gamma = \frac{\kappa_1 - \kappa_2}{\kappa_1 + \kappa_2} = 0.5,\\ &\Delta H = 40\,\mu\text{m}, \quad E = 5 \times 10^4\ \text{V/m}. \end{aligned} \tag{60}$$

It can be seen that the stress in the bilayer beam is uniform except for a small region near the crack tip and the two ends. This demonstrates that a beam with a sufficiently large length-to-thickness ratio can be taken as an infinite one.

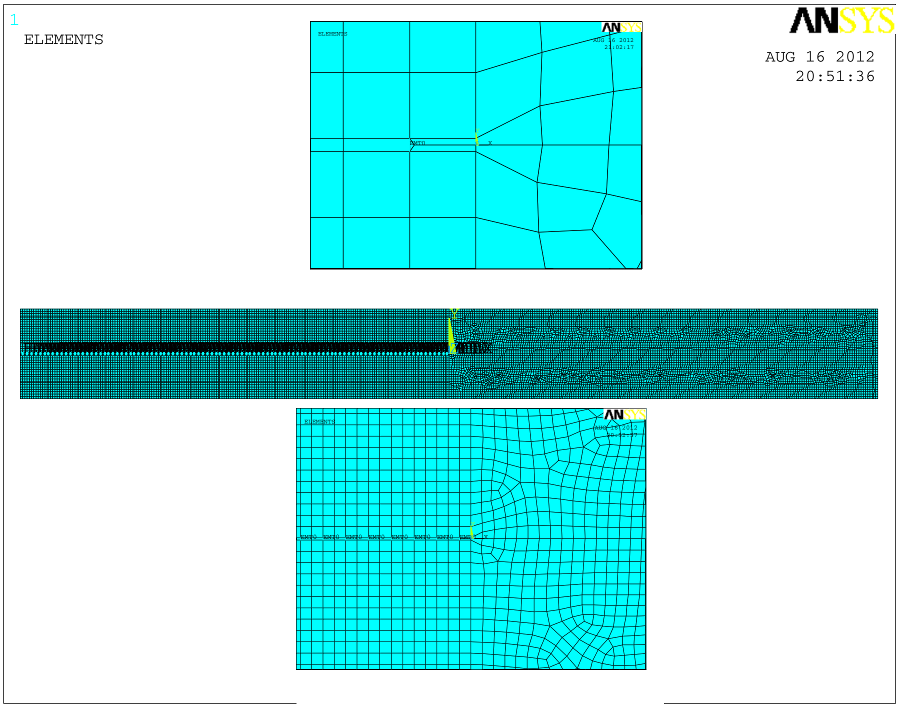

(a)

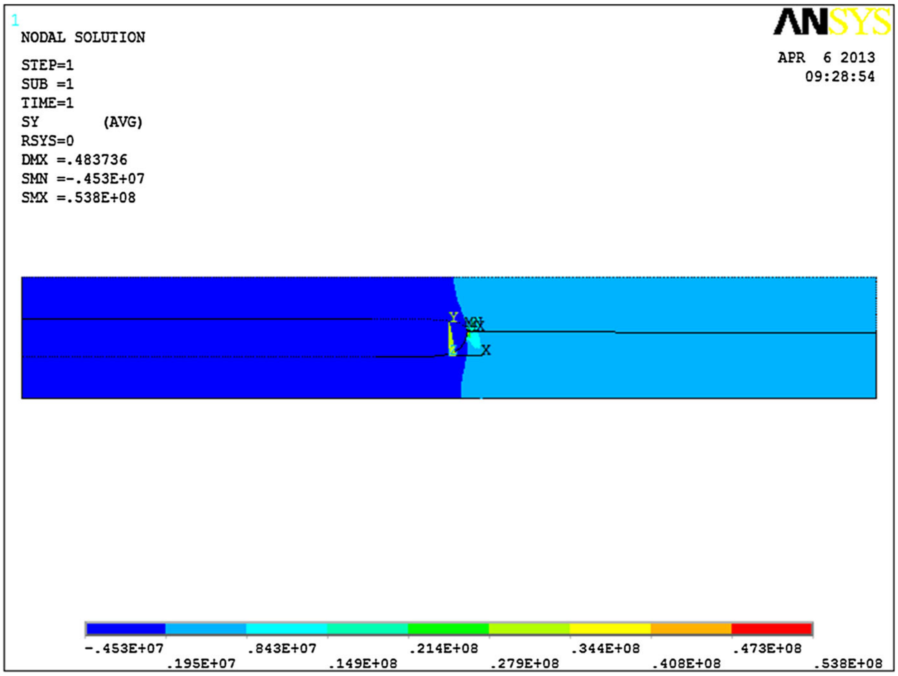

(b)

Fig. 8 **a** Finite element meshes. **b** Stress distribution in the bilayer beam by FEM

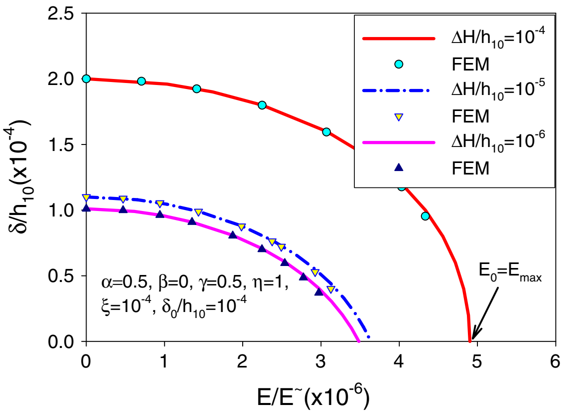

Fig. 9 The crack width versus the applied electric field strength under different mechanical loads

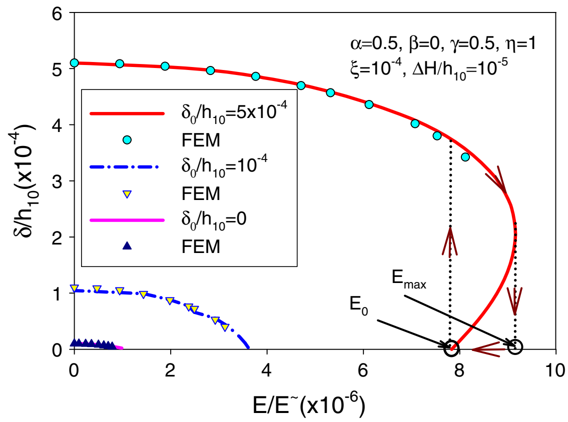

Fig. 10 The crack width versus the applied electric field strength for different values of the original crack width

In the following numerical calculations, we take $(V/h_{10})/E^{\sim}$, and $E^{\sim} = \sqrt{c_1/\kappa_1}$.

Figure 9 plots the normalized after-deformation gap versus the normalized applied electric field strength, $E/E^{\sim}$, under different mechanical loads $\Delta H/h_{10}$ with dielectric mismatch $\gamma = 0.5$, thickness ratio $\eta = 1$, normalized initial gap $\delta_0/h_{10} = 10^{-4}$ and normalized dielectric constant $\xi \equiv \kappa_c/\kappa_1 = 10^{-4}$. The elastic mismatch is described by the Dundurs parameters (Hutchinson and Suo 1992)

$$\alpha = \frac{\bar{c}_1 - \bar{c}_2}{\bar{c}_1 + \bar{c}_2},$$
$$\beta = \frac{1}{2}\frac{\bar{c}_1(1-\nu_1)(1-2\nu_2) - \bar{c}_2(1-\nu_2)(1-2\nu_1)}{\bar{c}_1(1-\nu_1)(1-\nu_2) + \bar{c}_2(1-\nu_2)(1-\nu_1)},$$
$$\bar{c}_i = Y_i/(1-\nu_i^2). \tag{61}$$

It can be seen that an applied electric loading pushes the notch to close. As shown in Fig. 9, the analytical solution based on Eq. (43a) is in excellent agreement with that from the FEM model also developed in this paper. It is also observed that for fixed V/h_{10}, δ/h_{10} increases with increasing mechanical loading $\Delta H/h_{10}$. We further note that, for other fixed parameters, when $\Delta H/h_{10} = 10^{-4}$, E_0 is almost equal to E_{max}. In other words, the threshold is about the same as the electric value which makes the gap being zero. When $E_0 = E_{\max}$, the $\delta - E$ curve intersects with the E-axis at an angle of 90°.

Figure 10 plots the after-deformation gap versus the applied electric field strength for different values of the initial gap, with $\delta_0 = 0$ corresponding to a crack. When the initial gap is sufficiently large, the threshold appears in the curve. For the case $\delta_0/h_{10} = 5 \times 10^{-4}$, we have $E_0/E^{\sim} = 830 \times 10^{-3}$(or $E_0 = 1.08 \times 10^6$ V/m) and $E_{\max}/E^{\sim} = 972 \times 10^{-3}$(or $E_{\max} = 1.26 \times 10^6$ V/m). In the region $E_0 < E < E_{\max}$, the solution has two branches. In one branch (i.e., the true physical solution in the upper part of the curve), the gap decreases with increasing applied electric field, whereas the other branch (also the second branch, i.e., the lower part of the curve) corresponds to one of two solutions of Eq. (40) satisfying $\delta > 0$. If the applied electric field exceeds E_{max}, the notch would close and the problem is then converted to an electric-field-induced sticky problem. For this case, the curve for the notch width versus the applied electric field under a given mechanical displacement shows a hysteresis loop, as discussed in detail by Zhang and Xie (2012).

Figure 11a, b show the influence of the elastic and dielectric mismatches, respectively, on the gap deformation. Figure 11a shows that for a fixed electric field and dielectric mismatch, δ/h_{10} decreases with increasing elastic mismatch α. Furthermore, a large electric field is required to reach the state of $\delta = 0$ when the elastic mismatch α is small (algebraically). Figure 11b plots the variation of δ/h_{10} vs. the normalized applied electric field $E/E^{\sim}$ for fixed elastic mismatch $\alpha = 0$ but with varying dielectric mismatch γ. It is observed from Fig. 11b that when $\alpha = 0$ and for a given electric field, δ/h_{10} increases with increasing dielectric mismatch γ, and that an increasing γ means that a large electric field is required to reach the state of $\delta = 0$. Figure 11b further shows the difference between the bilayer beam and the corresponding homogeneous beam

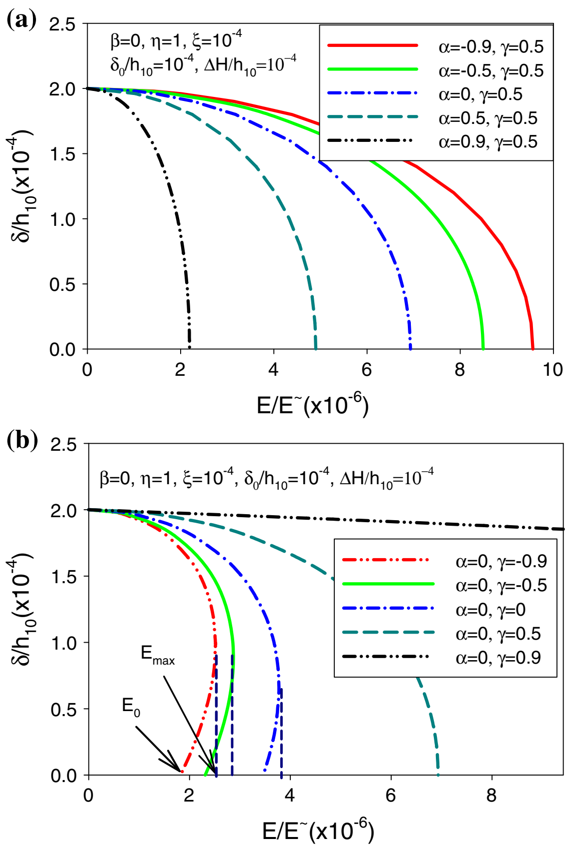

Fig. 11 The crack width versus the applied electric field strength with **a** different values of elastic mismatch, and **b** different values of dielectric mismatch

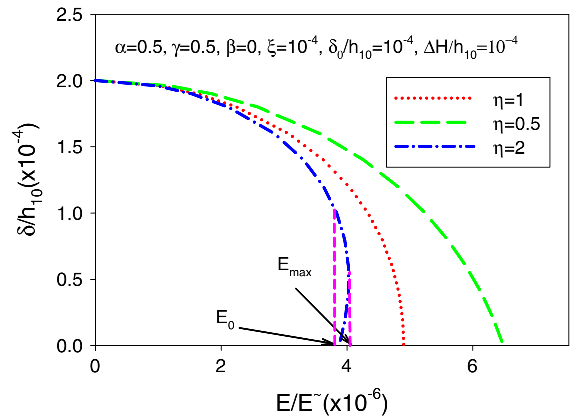

Fig. 12 The crack width versus the applied electric field strength with different thickness ratios of the two layers

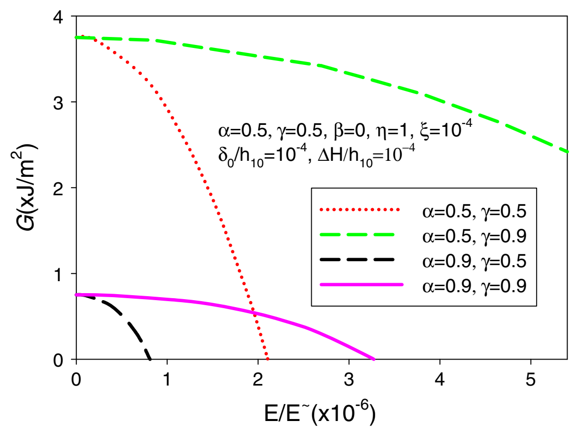

Fig. 13 Energy release rate versus the applied electric field strength

($\alpha = 0, \gamma = 0$), which actually provide us with the possibility of tuning the threshold behavior in the δ/h_{10} vs. V/h_{10} curve. In other words, a small (or negative) γ would imply an early threshold whilst a large (or positive) γ is associated with a late threshold (or even no threshold at all).

Figure 12 demonstrates the effect of the thickness ratio of the two layers $\eta = h_{10}/h_{20}$ on the after-deformation gap versus the applied electric field strength by the analytical approach. The fixed parameters are $\alpha = 0.5$, $\beta = 0, \gamma = 0.5$, $\xi = 10^{-4}$, $\delta_0/h_{10} = 10^{-4}$ and $\Delta H/h_{10} = 10^{-4}$. Figure 12 shows that, when other parameters are fixed and under a given electric field, δ/h_{10} decreases with increasing thickness ratio. This figure further shows that it is also possible to control the threshold behavior in the δ/h_{10} vs. $E/E^{\sim}$curve by changing the thickness ratio of the two layers of the beam.

Figure 13 plots the energy release rate of the notch in the bilayer beam. The result shows that the electric loading reduces the energy release rate, i.e., retards the crack propagation. It is very interesting to further observe from Fig. 13 that the energy release rate is more sensitive to the dielectric mismatch γ. In other words, for a fixed elastic mismatch α, the energy release rate decreases sharply with decreasing γ.

5 Concluding remarks

A nonlinear analytical solution considering the electrostatic tractions was derived for a bilayer dielectric beam model with a semi-infinite interfacial notch or crack under mechanical and electrical loading. In addition, a finite element method was developed and the finite element analysis was carried out to solve the same interfacial fracture problem. In the nonlinear finite element analysis, the deduced special TRANS126 element in ANSYS is successfully modified to simulate the electrostatic tractions. This new element would greatly broaden the application of finite element analyses to the failure of materials and structures under mechanical and electrical loadings. The numerical calculations verify the analytic results, indicating that both elastic and dielectric mismatches can greatly influence the energy release rate and other fracture behaviors. For a given mechanical load, there is a maximum tolerant electric field $E_{\max}$, at and beyond which the electrostatic tractions close the crack (notch). The conjugate of the maximum tolerant electric field is called the threshold of applied strain, at and below which the crack is closed due to the electrostatic tractions. The analysis and calculations exhibit also a pair of bifurcation field, E_0, and bifurcation strain. Under a given mechanical load, a hysteresis loop may occur in curves of crack width versus applied electric field in the range of $E_0 \leq E \leq E_{\max}$. These results are consistent with the previous investigations on the effects of electrostatic tractions on fracture of homogenous dielectrics (Zhang and Xie 2012).

Acknowledgments The work was supported by the National Natural Science Foundation of China (No. 11102186, No. 11072221, No. 11172273) and by Henan Province through the Bairen Program. TY Zhang was supported by the general research grant 622610 from the Hong Kong Research Grants Council, Hong Kong, China. The authors thank Mr. T. XIE for helping check the equations in the paper.

References

ANSYS® Academic Research, Release 11.0, Help System, Element Reference, TRANS126
England AH (1965) A crack between dissimilar media. J Appl Mech 32:400–402
Erdogan F (1965) Stress distribution in bonded dissimilar materials with cracks. J Appl Mech 36:650–652
Fan CY, Zhao MH, Meng LC et al (2011) On the self-consistent analysis, the energetically consistent approach, and electrostatic tractions in piezoelectric fracture mechanics. Eng Fract Mech 78:2338–2355
Gao CF, Tong P, Zhang TY (2004a) Effect of columbic force on piezoelectric fracture. Key Eng Mater 261–263:81–86
Gao CF, Zhao MH, Tong P et al (2004b) The energy release rate and the J-integral of an electrically insulated crack in a piezoelectric material. Int J Eng Sci 42:2175–2192
Hao TH, Shen ZY (1994) A new electric boundary condition of electric fracture mechanics and its applications. Eng Fract Mech 47:793–802
Hutchinson JW, Suo Z (1992) Mixed mode cracking in layered materials. Adv Appl Mech 29:63–191
Liechti KM, Chai YS (1990) Biaxial loading experiments for determining interfacial toughness. J Appl Mech 58:680–687
Landis CM (2004) Energetically consistent boundary conditions for electromechanical fracture. Int J Solids Struct 41:6291–6315
Li Q, Chen YH (2008) Why traction-free? Piezoelectric crack and coulombic traction. Arch Appl Mech 78:559–573
McMeeking RM (2004) The energy release rate for a Griffith crack in a piezoelectric material. Eng Fract Mech 71:1149–1163
Rice JR (1968) A path independent integral and approximation analysis of strain concentration by notches and cracks. J Appl Mech 35:379–386
Rice JR, Sih GC (1965) Plane problems of cracks in dissimilar media. J Appl Mech 32:418–423
Ricoeur A, Kuna M (2009) Electrostatic tractions at dielectric interfaces and their implication for crack boundary conditions. Mech Res Commu 36:330–305
Schneider GA (2007) Influence of electric field and mechanical sStresses on the fracture of ferroelectrics. Annu Rev Mater Res 37:491–538
Suo Z (1990) Singularities, interfaces and cracks in dissimilar anisotropic media. Proc R Soc Lond J Appl Mech 57:627–634
Suo Z, Hutchinson JW (1989) Interface crack between two elastic layers. Int J Fract 25:1337–1353
Suo ZG, Kuo CM, Barnett DM et al (1992) Fracture mechanics for piezoelectric ceramics. J Mech Phys Solids 40:739–765
Shapery RA, Davidson BD (1990) Prediction of energy release rate for mixed-mode delamination using classical plate theory. Appl Mech Rev 43:S281–S287
Tada H, Paris PC, Irwin GR (1985) The stress analysis of vracks handbook. Del Research, St. Louis, Missouri
Williams JG (1988) On the calculation of energy release rates for cracked laminates. Int J Fract 36:101–204
Xie T, Fan CY, Liu HT et al (2014) Effect of electrostatic tractions on the fracture behavior of a piezoelectric material under mechanical and/or electric loading. Theor Appl Fract Mech 69:6–16
Zhang TY, Gao CF (2004) Fracture behaviors of piezoelectric materials. Theor Appl Fract Mech 41:339–379
Zhang TY, Hack JE (1992) Mode III cracks in piezoelectric materials. J Appl Phys 71:5865–5870
Zhang TY, Qian CF, Tong P (1998) Linear electro-elastic analysis of a cavity or a crack in a piezoelectric material. Int J Solids Struct 35:2121–2149
Zhang TY, Xie T (2012) Effect of electrostatic tractions on the fracture behavior of a dielectric material under mechanical and/or electric loading. Sci China Technol Sci 55:2391–2403
Zhang TY, Zhao MH, Tong P (2002) Fracture of piezoelectric ceramics. Adv Appl Mech 38:147–289